ARIEL payload STOP analysis: a view on the in-flight operational cases for the telescope assembly

A. Brucalassi, J. A. Araiza-Durán, A. Tozzi, C. Galy, A. G. Perez, A. Caldwell, G. Morgante, D. Bruzzi, M. Caldwell, P. Chioetto, P. Eccleston, A. J. Fernandez Soler, D. Ferruzzi, D. Gottini, R. Lilli, G. Micela, E. Pace, E. Pascale, J. Perez Alvarez, R. Piazzolla, P. Picchi, G. Preti, M. Salatti, A. Scippa, G. Tinetti, P. Zuppella

Published version information:

Citation: A. Brucalassi et al., ARIEL payload STOP analysis: a view on the in-flight operational cases for the telescope assembly, Proceedings Volume 13092, Space Telescopes and Instrumentation 2024: Optical, Infrared, and Millimeter Wave; 130924L (2024)

DOI: https://doi.org/10.1117/12.3019257

ARIEL payload STOP Analysis: a view on the in-flight operational cases for the telescope assembly

A. Brucalassi[a], J. A. Araiza-Durán[a], A. Tozzi[a], C. Galy[b], A. G. Perez[c], A. Caldwell[d], G. Morgante[e], D. Bruzzi[d], M. Caldwell[d], P. Chioetto[f], P. Eccleston[d], A. J. Fernandez Soler[c], D. Ferruzzi[a], D. Gottini[a], R. Lilli[a], G. Micela[g], E. Pace[h], E. Pascale[i], J. Perez Alvarez[c], R. Piazzolla[l], R. Picchi[h], G. Preti[h], M. Salatti[l], A. Scippa[m], G. Tinetti[n], and P. Zuppella[f]

[a]INAF-Osservatorio Astrofisio di Arcetri, Largo E. Fermi 5, Firenze, Italy
[b]Centre Spatial de Liège, Univ. de Liège, Avenue du Pré-Aily, B4031 Angleur, Liège, Belgium
[c]Universidad Politécnica de Madrid, Plaza del Cardenal Cisneros 3, 28040 Madrid, Spain
[d]RAL Space, STFC Rutherford Appleton Laboratory, Didcot, Oxon, OX11 0QX, UK
[e]INAF-Osservatorio di Astrofisica e Scienza dello Spazio di Bologna, Via Piero Gobetti 93/3, 40129 Bologna, Italy
[f]CNR-Istituto di Fotonica e Nanotecnologie di Padova, Via Trasea 7, 35131 Padova, Italy
[g]INAF-Osservatorio Astronomico di Palermo, Piazza del Parlamento 1, 90134 Palermo, Italy
[h]Dip. Fisica ed Astronomia, Universita di Firenze, Largo E. Fermi 2, 50125 Firenze, Italy
[i]Dip. Fisica, La Sapienza Universita di Roma, Piazzale Aldo Moro 2, 00185 Roma, Italy
[l]ASI-Agenzia Spaziale Italiana, Via del Politecnico snc, Roma, Italy
[m]Dip. Ingegneria Industriale, Universita di Firenze, Via Santa Marta, 3 50139 Firenze, Italy
[n]Dept. Physics and Astronomy, Univ. College London, Gower Street, London WC1E 6BT, UK

ABSTRACT

Ariel (Atmospheric Remote-Sensing Infrared Exoplanet Large Survey) is the fourth medium-class mission (M4) of the ESA's *Cosmic Vision Program*. Its launch is planned for 2029. Ariel will observe a large and well selected sample of transiting gas giants, neptunes and super-earths around a wide range of host star types, with the objective to study planetary atmospheres and to understand composition and evolving processes of the planetary systems. A Structural, Thermal, and Optical Performance (STOP) analysis is conducted at Payload level to estimate the thermo-elastic induced degradation of the system performance for a number of selected environmental load cases. In particular, this document presents the general approach followed and the results of the optical design analysis performed to predict the performance of the Ariel Telescope Assembly for the in-flight operational cases during Cycle C-1.

Keywords: Ariel mission, STOP Analysis, Cassegrain Telescope, Aluminum mirror, Planet atmospheres

1. INTRODUCTION

The Atmospheric Remote-sensing Infrared Exoplanet Large-survey (Ariel) mission has been adopted by ESA as M4 mission in the framework of the ESA 2015-2025 *Cosmic Vision Program*. Its launch is planned for 2029. Ariel will observe a large and well selected sample (∼1000) of transiting gas giants, Neptunes and Super-Earths around a wide range of host star types, with the objective to address the fundamental questions on what exoplanets are made of and how planetary systems form and evolve.[1–3] Ariel will perform primary and secondary transit spectroscopy in the 1.10 to 7.80 micron spectral range and broad-band photometry in the Optical (0.50 - 0.80 micron) and Near IR (0.80 - 1.10 micron) ranges with an off-axis Cassegrain telescope having a 1.1x0.7 m primary mirror and two main instruments AIRS, the Ariel Infrared Spectrometer, and the Fine Guidance System (FGS).

Further author information: (Send correspondence to anna.brucalassi@inaf.it)
Anna Brucalassi.: E-mail: anna.brucalassi@inaf.it, Telephone: +39 055 2752-329
Andrea Tozzi: E-mail: andrea.tozzi@inaf.it, Telephone: +39 055 2752-288

Space Telescopes and Instrumentation 2024: Optical, Infrared, and Millimeter Wave, edited by Laura E. Coyle, Shuji Matsuura, Marshall D. Perrin, Proc. of SPIE Vol. 13092, 130924L · © 2024 SPIE · 0277-786X · doi: 10.1117/12.3019257

A Structural, Thermal, and Optical Performance (STOP) analysis is conducted at Payload level to estimate the thermo-elastic induced degradation of the system performance for a number of selected environmental load cases. In particular, this document describes the general approach followed and shows the results of the optical design analysis done to predict the performance of the Ariel Telescope Assembly (including the Bipods Model and the Service Module Interface) for the in-flight operational cases during Cycle C-1.

The Ariel STOP analysis is performed by a team of institutes across the Ariel Consortium[4] and the responsibilities are allocated as shown in Table 1.

Table 1. Distribution of the different responsibilities for the Ariel STOP analysis.

Institution	**Responsibilities**
Space RAL	Case Definition. Management and overview of cycles. Maintains payload optical model and assess Com. Optics displacements. Maintains CAD and FEM configurations.
INAF	Flight case performance analysis. Payload thermal analysis. Telescope optical model management.
CSL	Ground case performance analysis.
UPM	STOP FEM analysis. Telescope mechanical and thermal model management.

2. WORKFLOW OVERVIEW

Different Cycles (or analysis runs) are generally completed before a payload review. For each of the cycles a controlled number of changes are made to all of the involved models (CAD, Finite Element Model (FEM), Thermal Mathematical Model (TMM), Optical, Performance) to allow the latest stage of the payload design to be incorporated.[5–7]

At each cycle, a number of *Cases* are defined to identify key scenarios to be analysed. Moreover, specific operational In-Flight cases and Ground test cases have been selected as a verification between the analyses presented by INAF and the analysis made by CSL. A summary of the in-flight cases for Cycle C-1 is given in Fig. 1.

3. OPTICAL MODEL

The general description of the Telescope Optical model is presented in the following. The system is an off-axis Cassegrain telescope (M1, M2) followed by a re-collimating off-axis parabola (M3), a plane fold mirror (M4), a second plane fold mirror (M5) and a dichroic beam-splitter (D1) that divides the beam into the FGS and IR spectrometer channels. M1, M2 and M3 share a common optical axis, which lies parallel to the X-payload axis. After D1, a second dichroic D2 splits the beam into the two IR spectrometer channels. The beam in each channel is brought to a focus at the spectrometer slit by a pair of identical off-axis parabolas, M7 Ch0 and M7 Ch1. An additional fold mirror, M6 is included in the Ch0 path.

Fig. 2 shows the Telescope optical layout along with the optical coordinate system (XOPT, YOPT, ZOPT). The origin is located at the vertex of the parent parabola for M1. The direction of the telescope optical axis (defined by the common M1, M2 and M3 optical axis) is parallel to the X ARIEL-payload axis. The telescope pointing axis, or line of sight (LOS), is offset by 0.1deg with respect to the telescope optical axis to give an accessible return beam from M3. The 50K system aperture stop (an ellipse with major axis dimensions of 1100 mm x 730 mm) is at the M1 surface. M4 is positioned to direct the beam onto the telescope optical bench such that all subsequent beams at the centre of the field lie in a plane parallel to the tangent plane to the mirror surface. The chief ray at the centre of the field is at 275 mm from the tangent plane to the mirror surface. The

ID	Case name	Displ	Str	The	Opt	Comment
	Nominal CAD Design Case					Baseline design
00	**Homothetic load case**		Y		G, F	Comparison baseline
01	**Uniform Cooldown Case**	Y	Y		G, F	Uniform temperature at 50 K
02	**SVM displacement at RT**	Y	Y		F	Uniform ambient
03	**Hot Operational Case - SVM Uniform**	Y	Y	Y	F	Hot rad. & uniform cond. I/F
04	**Hot Operational Case - SVM Gradient**	Y	Y	Y	F	Hot rad. & gradient cond. I/F
05	**Cold Operational Case - SVM Uniform**	Y	Y	Y	F	Cold rad. & uniform cond. I/F
05b	**Representative offset sensitivity case**	Y	Y	Y	F	Cold rad. & uniform cond. I/F
06	**Cold Operational Case - SVM Gradient**	Y	Y	Y	F	Cold rad. & gradient cond. I/F
07	**Transient End state (after 10 hrs)**	Y	Y	Y	F	10 K drift from Hot Op Case
07.1	**Transient End state (after 10 hrs)**	Y	Y	Y	F	10 K drift from Hot Op Case
07a	**Slew End state (after S/C slew)**	Y	Y	Y	F	0.5 K drift from Hot Op Case
07a.1	**Slew End state (after S/C slew)**	Y	Y	Y	F	0.5 K drift from Hot Op Case

Figure 1. STOP analysis in-flight case summary for cycle C1.

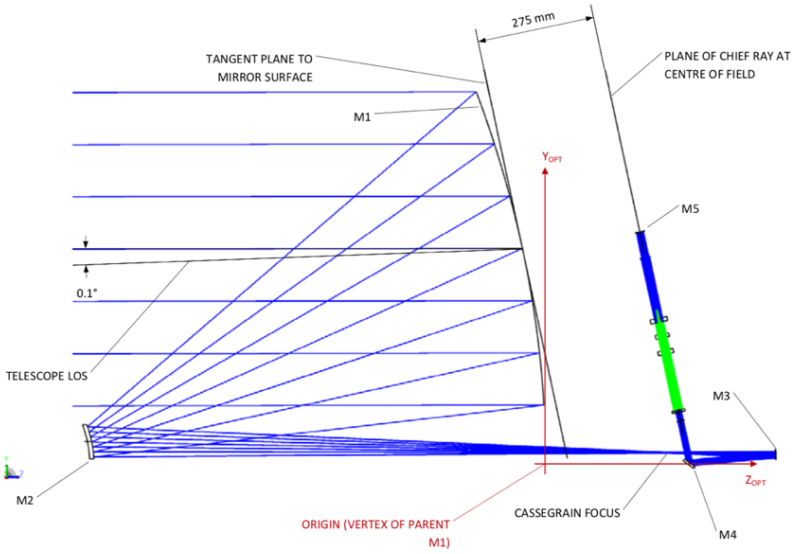

Figure 2. Telescope-view drawing in the Y_{opt}-Z_{opt} plane

beam on the optical bench has its major axis parallel to the plane of the optical bench. The beam dimensions on the optical bench are 20 mm x 13.3 mm.

Two different optical prescriptions have been defined:

- **Operational Temperature Optical Model, 50K and 0 ATM.**
  This model is the perfect optical model as defined during the design phase.
- **Room Temperature Model, 293K and 1 ATM.**
  This model has been scaled up from 50K for the assembly and alignment purpose at room temperature. A 293 K STOP model is generated to be incorporated into the Payload CAD.

During the previous analysis cycle, has been defined that the initial starting point for the STOP analysis should be the Room Temperature Model. The different impacts will be assessed and compared with the initial

performances and geometrical properties of this model.

3.1 Exit Pupil and Dummy Surface Definition

In order to track the performances during the STOP analysis, two additional elements are included in the thermo-elastic analysis (see Fig. 3):

1. The Intermediate Pupil Stop (IPS) to represent the initial exit pupil.
2. A Dummy element to track the back of the M1 aperture centre with respect to the telescope output beam on the Telescope Optical Bench (TOB). This dummy element is chosen to represent the M5 mirror centre as defined in the optical design prescription. It is located at a distance from the TOB such that the vector from IPS centre to the M5 dummy is parallel to the TOB itself (for the Room Temperature Model at 293K and 1 ATM).

Those additional elements are materialized with aluminum blocks 50 mm x 50 mm and 10 mm thick rigidly attached to the TOB.

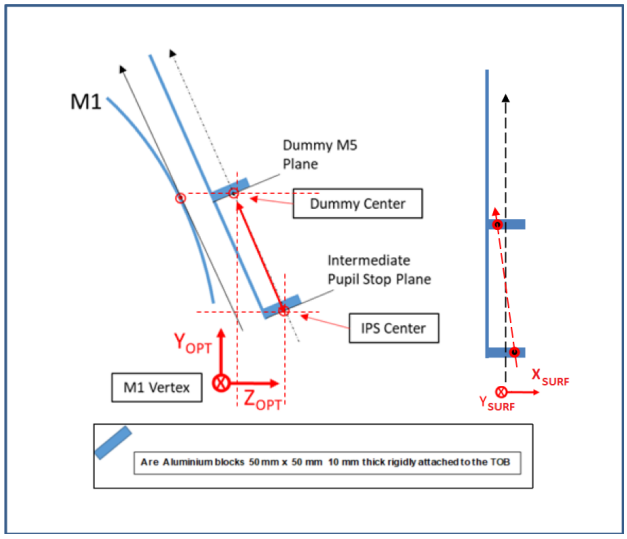

Figure 3. IPS and Dummy Surface definition

4. PERFORMANCE MODEL

The work plan followed during the STOP analysis is presented in the flowchart shown in Fig. 4 and is based on four critical steps:

- **Verification step:** between the FEM model and Optical model as part of the performance model. This includes a check of the Warm Optical Model to the Cold FEM isothermal through the Sigfit software* and the optical software used.
- **Validation step:** Two of the cases are used as a validation between CSL and INAF analysis of the Ground and Flight Cases.
- **Optical impact analysis:** The FEM deformations for all the cases are imported through SigFit inside the optical model and evaluated according to the performance metrics.
- **Compensation analysis:** Once the optical impacts are identified, the STOP analysis will concentrate on the possible ways to compensated these impact and retrieve nominal performances.

*https://sigmadyne.com/

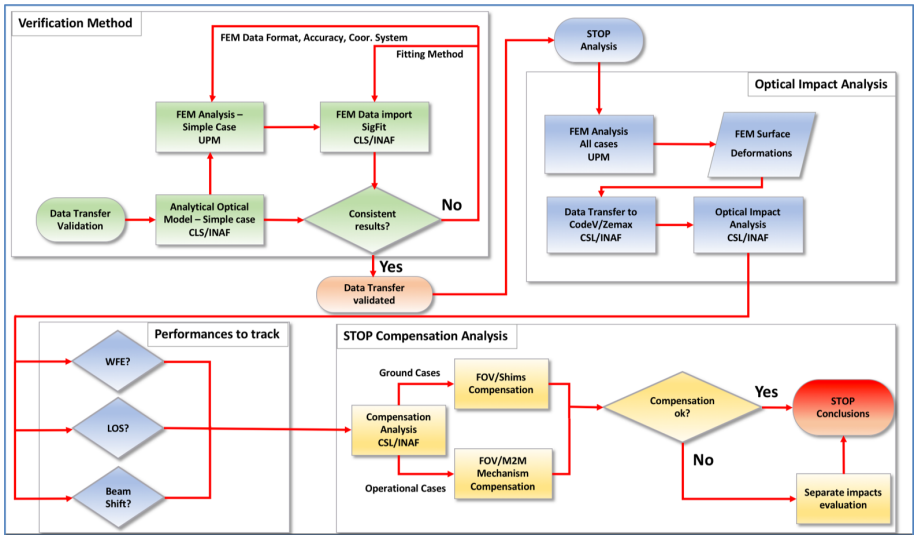

Figure 4. STOP analyses flowchart. For CSL: CODE V Optical Design Software (https://www.synopsys.com/optical-solutions/codev.html). For INAF: Ansys Zemax OpticStudio (https://www.ansys.com/it-it/products/optics/ansys-zemax-opticstudio).

4.1 PERFORMANCE METRICS

In both the flight and ground performance modelling, the following performances are tracked as outputs to be optimised with the compensation measures.

4.1.1 WaveFront Error

The WaveFront Error (WFE) is measured and optimized for all STOP cases. This WaveFront Error is measured at the exit pupil plane, which changes depending on the system perturbation and for all entrance fields defined: the worst RMS value is reported. A Zernike decomposition is provided for the best compensation cases, and the PSF is also provided in order to compute the associated Encircled Energy distribution.

The Zernike polynomial definition used in this document is described in R. Noll "Zernike polynomials and atmospheric turbulence", J. Opt. Soc. Am., Vol.66, No 3, p207 (1976).

4.1.2 Chief Ray Angle

In the initial design, the exit pupil will be considered as a physical diaphragm that will move during the thermal and elastic transitions. This pupil will be defined as "Intermediate Pupil Stop" (IPS) in all the STOP analysis. Per definition and design for the unperturbed telescope, the exit pupil matches the IPS. Per definition, the chief ray hits the IPS plane and the Dummy (M5) surface plane at their center.

In the perturbed design the IPS and Dummy element will move due to thermo-elastic deformation. The real exit pupil location will depend on the new optical configuration due to thermo-elastic deformation, and the chief ray angle inside this new exit pupil plan will differ from the angle defined by the new location of the IPS and Dummy plane. The Chief Ray Angle corresponds to the inclination of the line that goes from the point representing the intersection of the Chief Ray at the surface IPS to the point where the Chief Ray crosses surface Dummy M5 (see Fig. 3).

4.1.3 Pupil and Beam Shift

The IPS and Dummy surface define the new mechanical TOB after deformation. As the beam exiting the telescope is meant to enter the next instrument by going through the M5 mirror (not defined here), the last parameter that was defined useful to track was the spatial shift of the beam along the TOB. In particular, this spatial shift will be useful to know the potential vignetting that can occur at the M5 mirror is all the cases.

M1 Mirror	Temp_Change 50K Analytical (ZEMAX) mm			Z_NAS_50K FEM	Difference 50K Analytical vs FEM
Node #	X_ZMX_50K	Y_ZMX_50K	Z_ZMX_50K Analytical	(mm)	(nm)
400000	-3,492105E-02	-136,58893	-3,95689	-3,956880838	9,16210
402184	-2,852014E+02	649,68180	-108,52569	-108,5256931	3,12000
401670	1,691869E+02	386,13394	-38,31261	-38,31261962	9,62400
403194	-7,941346E+01	436,33132	-42,4016000	-42,4016045	4,49700
403249	-2,554328E+02	497,51720	-67,42496	-67,42496851	8,51200
403331	-2,174406E+02	693,78576	-113,9566	-113,9566076	7,55000
403394	-1,281633E+02	315,93546	-25,05856000	-25,05856574	5,73800

Figure 5. Random node data verification.

4.2 COMPENSATORS

In both the in-flight and ground performance modelling, the following compensation measures are available to the analysis to recover the tracked performance, shown in the next section.

4.2.1 Operational Cases

In the thermo-elastic considered cases, the compensation analysis foresees that it will be applied in operation. To that aim, the only physical parameters available are those of the **M2 Mirror Mechanism (M2MM)**. The considered ranges are those defined in the M2MM specifications:

- $\pm 350 \mu$m transaltion along Z axis.
- $\pm 2000 \mu$rad X and Y tip-tilt ($\pm$412.5arcsec).

These movements are applied at the M2MM movement origin, which is not located at the M2 mirror vertex.

Additionally, another compensation parameter will be the **FoV offset**, which is identified as an additional offset to the initial FoV. In particular, the center field is set to hit the M1 mirror with an initial angle of 0.1deg. This angle can be set as a variable to help with the compensation.

4.2.2 Ground Cases

For the static ground test at ambient the compensation considered is a shimming of the M2 mirror. This compensation is considered to be applied at its vertex:

- $\pm$3mm in the XOPT/YOPT/ZOPT direction (M2).
- In some cases, a compensation of $\pm$2arcdeg around XOPT is introduced.

FoV compensation as defined for the Operational cases.

5. RESULTS

In the following are summarized the results for the in-flight cases at operational temperature 50K analyzed in this document, under different configurations of the Telescope Assembly orientation.

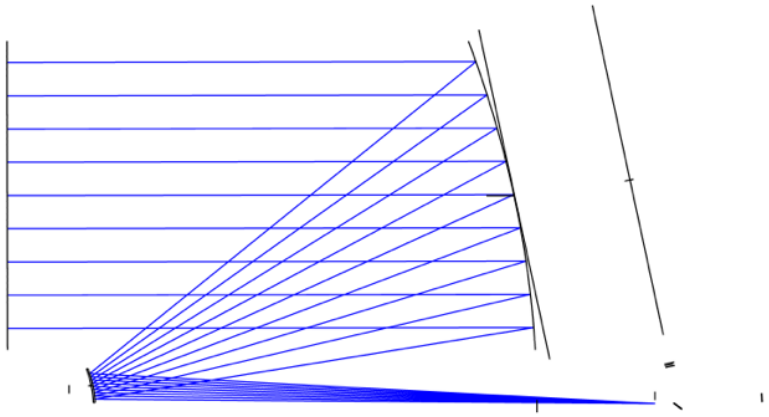

Figure 6. 3D layout of the uncorrected Case01.

5.1 DATA TRANSFER VERIFICATION: 50K ISOTHERMAL CASE

The first major step of the STOP analyses is to establish and verify a translation process between the FEM analysis made by UPM and the Zemax optical design. A correct translation will ensure a correct assessment of the optical impact. In order to do that, a simple case is defined, which could be analytically described in the optical software. The hypotheses of this simple case are the following:

- All aluminum telescope and structure
- No bipods constraints
- Uniform temperature excursion from 293K to 50K
- Uniform CTE of $1.67593648 \cdot 10^{-5}$ K^{-1}

The analytical contraction is computed to describe the temperature transition in Zemax. The results were compared with the equivalent case obtained by the FEM analysis and translated into optical prescription to be used in Zemax using SigFit software. It has been established that the Axial-Sag non-Linear translation method gives results accurate enough to assess the optical impact of FEM analysis cases.
The first verification and iterations is made analytically with random nodes verification as described by Fig. 5.

It is verified that initial surfaces and degraded surfaces are well described and sufficiently accurate between FEM prescription and Zemax ones (see first green column below). Finally, the simple case is successfully translated into Zemax and the comparison of the WFE maps shows a completely equivalent WFE. (Down to the nm accuracy).

5.2 IN-FLIGHT OPERATIONAL CASES

Among the different in-flight cases at operational temperature 50K analyzed, in this work we will present in details an example corresponding to a specific configuration of the Telescope Assembly, the other results will be summarized in a final table.

5.2.1 CASE01: Thermoelastic at 50K

The analysis evaluates the thermoelastic deformation from initial state (reference design at 293K and with no applied loads) to State 01 (uniform temperature distribution at 50K) with fixed Service Module (SVM) interfaces.

This is one of the two cases that have been also selected to be run in parallel by INAF and CSL institutes in order to control and validate the analysis made using CodeV (CSL) and using Ansys Zemax OpticsStudio (INAF). The second validation analysis is done using a ground case, not described in this paper.

Inputs: Temperature and boundary conditions for this analysis are the following: Uniform temperature distribution at 50K. No gravity load. Presence of Bipods to constrain the interfaces (fixed SVM IFs).

FEM deformation impact: The raw importation of the deformation gives the results described below in Fig. 6. The uncorrected case is completely scrambled: the M4 Mirror back stops the beam.

Compensation: Fig. 7 shows the results with the compensation applied using both M2MM and FoV offset. Fig. 8 shows the WFE rms for all the fields of Case01 compensated with M2MM and FoV offset.

	Nominal	FC .Diff [asec|um]	
LoS X [Deg]	0.1	0.169	-249.308
LoS Y [Deg]	0.0	-0.001	2.563
M2M Sh-Z [mm]	0.0	-0.086	86.187
M2M TltX [Deg]	0.0	-0.100	361.274
M2M TltY [Deg]	0.0	-0.007	23.735
M2M Sh-X [mm]	0.0	0.000	0.000
M2M Sh-Y [mm]	0.0	0.000	0.000

Figure 7. Compensation Parameters with MM2M and FoV offset for Case01.

	FoV X [asec]	FoV Y [asec]	RMS WFE [nm]	RMS WFE TR [nm]
Field 01	0.00	0.00	75.87328	53.72206
Field 02	10.44	10.44	75.48302	55.59333
Field 03	10.44	-10.44	76.00540	53.09983
Field 04	0.00	15.12	76.89693	57.27967
Field 05	0.00	-15.12	74.22365	53.78057
Field 06	15.12	0.00	74.73330	53.44719
Field 07	-10.44	10.44	76.59533	55.95747
Field 08	-10.44	-10.44	76.09686	53.69677
Field 09	-15.12	0.00	71.60665	54.24913

Figure 8. WFE RMS for all the fields for Case01 compensated with M2MM and FoV offset.

Fig. 9 illustrates the corresponding WFE maps (Piston, Tip/Tilt and focus removed) for Center Field in the case of the Fully Compensated system (FC) at the exit pupil and for M1 mirror alone.

Fig. 10 below illustrates the associated Pupil/Beam (P/B) Shift, the Chief Ray Angle and the TOB Angle at IPS for the compensation of Case01 with M2MM and FoV offset.

Finally, the application of M2M and FoV offset compensates the beam shift and retrieves the WFE at the level of M1 values, compliant with the requirements.

Fig. 11 below gives an illustration of the PSF output for 3000nm and 500nm. This is just an output and not optimised for during the analysis.

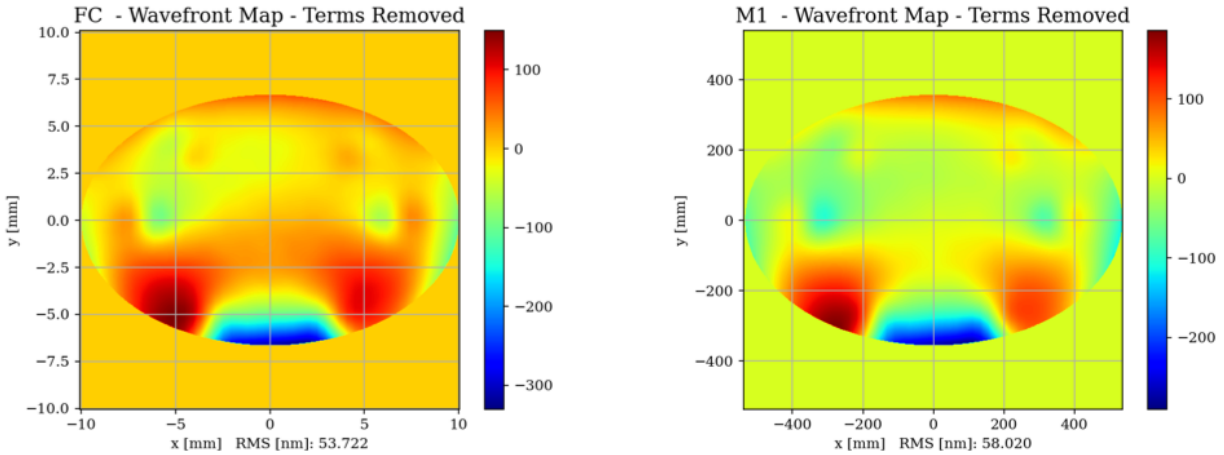

Figure 9. Left: Full compensated WFE map at the Exit Pupil. Right: M1 WFE map. Piston, Tilts and Focus terms removed.

	Values
P/B IPS Shift X [um]	-3.12038
P/B IPS Shift Y [um]	4.52285
P/B DM5 Shift X [um]	-3.12862
P/B DM5 Shift Y [um]	4.53067
ChR Angle X [asec]	0.00379
ChR Angle Y [asec]	-0.00360

	Nominal	FC .	Diff [asec]
TOB X [Deg]	0.000	0.000	-0.067
TOB Y [Deg]	12.165	12.244	-282.324

Figure 10. Top panel: Pupil/Beam Shift (P/B) and Chief Ray Angle for Case01 compensated with M2MM and FoV offset. Bottom panel: Telescope Optical Bench Angle (TOB) for Case01 compensated with M2MM and FoV.

5.2.2 In-Flight STOP Cases Summary

Fig. 12 presents a summary of all the compensation trials and their associated performance used during the cycle C-1 for the in-flight STOP analyses cases. During this analysis, it has been confirmed that the thermal effects and the bipods displacements have important impacts on the in-flight operational performances of the telescope, although the use of the FoV and the M2MM compensators allows the TA WFE to be recovered and brought back to the WFE values of M1 mirror.

6. CONCLUSIONS

The aim of the STOP analysis is to assess the thermoelastic impact of the operational In-Flight and Ground test environments onto the telescope model. This document presents the results of the optical design analysis performed by INAF to predict the performances of the Ariel Telescope Assembly for the operational In-Flight cases of Cycle C-1. The analysis is done using Ansys Zemax OpticStudio tool. The Data Transfer Validation process confirms a coherent analytical contraction. The different In-Flight Cases studied show important impacts of the thermal effects and bipods displacements on the TA WFE performances.

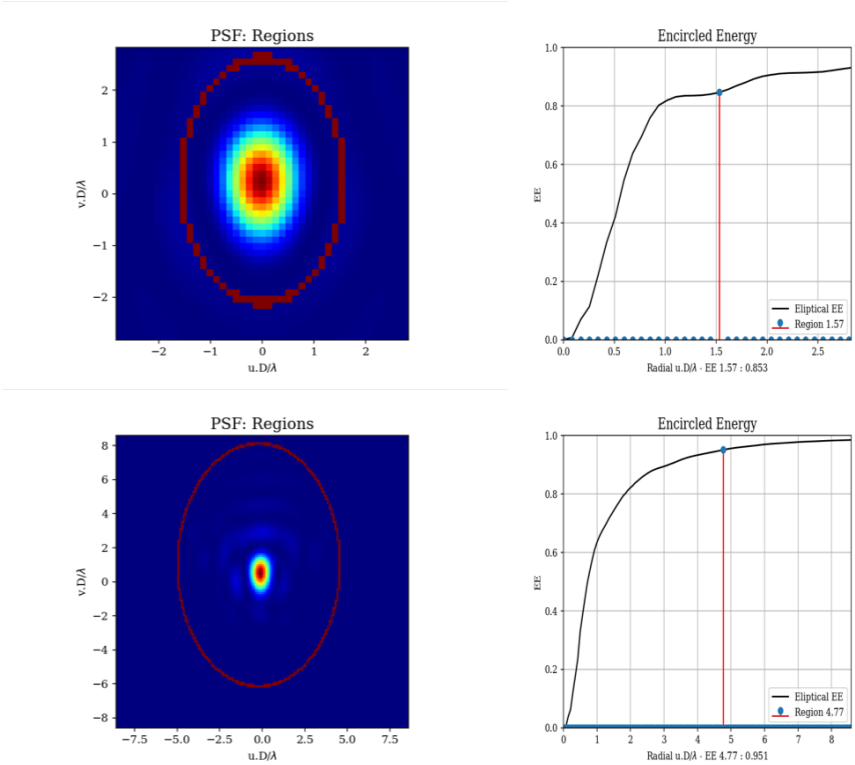

Figure 11. Top: PSF and Encircled Energy at 3000nm. Bottom: PSF and Encircled Energy at 500nm.

ACKNOWLEDGMENTS

This activity has been realized under the Implementation Agreement n. 2021-5-HH.0 of the Italian Space Agency (ASI) and the National Institute for Astrophysics (INAF) Framework Agreement "Italian Participation to Ariel mission phase B2/C".

	Case02	Case03	Case04	Case05	Case06	Case07.1	Case07	Case07a.1	Case07a
Compensator:									
LOS X Tilt [asec]	37,14211	10,66358	-277,312	-215,829	-217,086	-250,004	-213,25	-251,721	-222,569
LOS Y Tilt [asec]	-0,99431	-0,89221	2,11921	1,60204	1,59674	12,2743	1,97779	16,78497	1,9096
M2MM Z Shift [um]	-2,69325	1,52657	16,0175	17,5932	17,05122	15,57348	10,05033	16,21231	10,38512
M2MM X Tilt [asec]	-13,5293	15,27024	68,55742	88,05984	83,96662	64,61042	19,66123	70,66674	23,43468
M2MM Y Tilt [asec]	25,00065	25,9047	52,28409	48,3983	48,34882	76,73745	50,90568	87,339	50,43486
M2MM X Shift [um]	0	0	0	0	0	0	0	0	0
M2MM Y Shift [um]	0	0	0	0	0	0	0	0	0
P/B Shift:									
ChR X @ DM5 [um]	-3,01981	-3,13926	-6,63176	-5,99188	-5,83633	-10,104	-6,62348	-11,7015	-6,49004
ChR Y @ DM5 [um]	-1,3532	1,84293	-41,746	-36,2247	-36,9008	-41,8116	-46,707	-40,6392	-45,9318
ChR X @ IPS [um]	-3,02001	-3,13953	-6,64121	-5,97563	-5,83214	-10,1107	-6,63953	-11,6867	-6,47995
ChR Y @ IPS [um]	-1,35165	1,84453	-41,7626	-36,231	-36,8917	-41,8453	-46,7796	-40,6458	-45,8999
ChR Ang X [asec]	0,00009	0,00012	0,00435	-0,00748	-0,00193	0,00311	0,00739	-0,00681	-0,00465
ChR Ang Y [asec]	-0,00071	-0,00073	0,00765	0,00291	-0,0042	0,01552	0,03342	0,00306	-0,01471
TOB Y:									
Init Angle [Deg]	12,16509	12,16509	12,16509	12,16509	12,16509	12,16509	12,16509	12,16509	12,16509
Def. Angle [Deg]	12,15444	12,16265	12,23965	12,22391	12,2241	12,23194	12,22042	12,23262	12,22313
Change [asec]	38,34174	8,79219	-268,429	-211,762	-212,42	-240,649	-199,187	-243,107	-208,94
Total Energy:									
TE [%]	66,67333	66,67333	66,59341	66,59341	66,59341	66,59341	66,6034	66,59341	66,61339

	Case02	Case03	Case04	Case05	Case06	Case07.1	Case07	Case07a.1	Case07a
WFE Maps:									
FC RMS [nm]	6,3513	273,5952	272,051	211,1976	212,6587	273,3818	281,6837	275,9289	279,8544
FC RMS RT [nm]	3,56707	99,9094	99,04666	78,48637	79,81591	100,4239	102,7353	100,7888	102,1285
M1 RMS [nm]	3,28385	265,4244	263,5131	200,8302	204,4912	265,4409	269,0112	265,0308	269,0364
M1 RMS RT [nm]	2,753	102,4139	101,5757	82,56417	83,83552	103,0029	104,3701	102,9326	104,1343
IF RMS [nm]	66,31104	321,1477	317,9893	254,9449	257,2638	318,1334	325,6677	321,6824	322,7248
IF RMS RT [nm]	43,22056	96,7808	95,98128	76,88792	78,22356	97,72502	99,25032	97,8544	98,98191
Actuators:									
Act [um]	345,0574	318,5507	318,0135	317,6246	318,1817	310,9888	324,4017	307,112	324,2107
Act [um]	360,0898	324,9353	323,833	316,5054	318,1225	329,0554	342,5231	328,4336	341,1183
Act [um]	352,9326	359,908	360,101	363,0904	362,5422	363,2354	352,9242	365,8175	353,5156
IntFocus Position:									
GC - X [mm]	-0,04627	-0,04572	-0,04569	-0,04582	-0,04567	-0,08646	-0,04586	-0,10484	-0,04578
GC - Y [mm]	24,50824	25,51144	25,51051	25,4409	25,44536	25,4799	25,44261	25,50094	25,46671
GC - Z [mm]	280,2963	278,8391	278,8382	278,9706	278,9698	278,8399	278,9952	278,7989	278,968
ExitP Position:									
GC - X [mm]	-0,04718	-0,05032	-0,05034	-0,04988	-0,04971	-0,09328	-0,05035	-0,11257	-0,05018
GC - Y [mm]	97,99611	98,75727	98,72338	98,63032	98,75807	98,72048	98,66533	98,70888	98,59928
GC - Z [mm]	315,3784	313,6897	313,6953	313,8415	313,8144	313,7001	313,8809	313,6642	313,8686
ParaxialL Spot:									
CenRay - X [mm]	0,00945	0,00937	0,00936	0,0094	0,0094	0,0082	0,00937	0,00767	0,00937
CenRay - Y [mm]	-0,04451	0,31141	0,31243	0,2465	0,24727	0,2801	0,23183	0,28297	0,24324
S GC - X [mm]	0	0	0	0	0	0	0	0	0
S GC - Y [mm]	332,779	333,8565	333,8558	333,7482	333,7529	333,8197	333,7413	333,849	333,7724
S GC - Z [mm]	264,8361	264,6038	264,604	264,6272	264,6262	264,6118	264,6287	264,6055	264,622

Figure 12. STOP Cases summary – In-Flight Operational cases.

REFERENCES

[1] Tinetti, G., Drossart, P., Eccleston, P., Hartogh, P., Heske, A., Leconte, J., Micela, G., Ollivier, M., Pilbratt, G., Puig, L., Turrini, D., Vandenbussche, B., Wolkenberg, P., Beaulieu, J.-P., Buchave, L. A., Ferus, M., Griffin, M., Guedel, M., Justtanont, K., Lagage, P.-O., Machado, P., Malaguti, G., Min, M., Nørgaard-Nielsen, H. U., Rataj, M., Ray, T., Ribas, I., Swain, M., Szabo, R., Werner, S., Barstow, J., Burleigh, M., Cho, J., Coudé du Foresto, V., Coustenis, A., Decin, L., Encrenaz, T., Galand, M., Gillon, M., Helled, R., Morales, J. C., García Muñoz, A., Moneti, A., Pagano, I., Pascale, E., Piccioni, G., Pinfield, D., Sarkar, S., Selsis, F., Tennyson, J., Triaud, A., Venot, O., Waldmann, I., Waltham, D., Wright, G., Amiaux, J., Auguères, J.-L., Berthé, M., Bezawada, N., Bishop, G., Bowles, N., Coffey, D., Colomé, J., Crook, M., Crouzet, P.-E., Da Peppo, V., Sanz, I. E., Focardi, M., Frericks, M., Hunt, T., Kohley, R., Middleton, K., Morgante, G., Ottensamer, R., Pace, E., Pearson, C., Stamper, R., Symonds, K., Rengel, M., Renotte, E., Ade, P., Affer, L., Alard, C., Allard, N., Altieri, F., André, Y., Arena, C., Argyriou, I., Aylward, A., Baccani, C., Bakos, G., Banaszkiewicz, M., Barlow, M., Batista, V., Bellucci, G., Benatti, S., Bernardi, P., Bézard, B., Blecka, M., Bolmont, E., Bonfond, B., Bonito, R., Bonomo, A. S., Brucato, J. R., Brun, A. S., Bryson, I., Bujwan, W., Casewell, S., Charnay, B., Pestellini, C. C., Chen, G., Ciaravella, A., Claudi, R., Clédassou, R., Damasso, M., Damiano, M., Danielski, C., Deroo, P., Di Giorgio, A. M., Dominik, C., Doublier, V., Doyle, S., Doyon, R., Drummond, B., Duong, B., Eales, S., Edwards, B., Farina, M., Flaccomio, E., Fletcher, L., Forget, F., Fossey, S., Fränz, M., Fujii, Y., García-Piquer, Á., Gear, W., Geoffray, H., Gérard, J. C., Gesa, L., Gomez, H., Graczyk, R., Griffith, C., Grodent, D., Guarcello, M. G., Gustin, J., Hamano, K., Hargrave, P., Hello, Y., Heng, K., Herrero, E., Hornstrup, A., Hubert, B., Ida, S., Ikoma, M., Iro, N., Irwin, P., Jarchow,

C., Jaubert, J., Jones, H., Julien, Q., Kameda, S., Kerschbaum, F., Kervella, P., Koskinen, T., Krijger, M., Krupp, N., Lafarga, M., Landini, F., Lellouch, E., Leto, G., Luntzer, A., Rank-Lüftinger, T., Maggio, A., Maldonado, J., Maillard, J.-P., Mall, U., Marquette, J.-B., Mathis, S., Maxted, P., Matsuo, T., Medvedev, A., Miguel, Y., Minier, V., Morello, G., Mura, A., Narita, N., Nascimbeni, V., Nguyen Tong, N., Noce, V., Oliva, F., Palle, E., Palmer, P., Pancrazzi, M., Papageorgiou, A., Parmentier, V., Perger, M., Petralia, A., Pezzuto, S., Pierrehumbert, R., Pillitteri, I., Piotto, G., Pisano, G., Prisinzano, L., Radioti, A., Réess, J.-M., Rezac, L., Rocchetto, M., Rosich, A., Sanna, N., Santerne, A., Savini, G., Scandariato, G., Sicardy, B., Sierra, C., Sindoni, G., Skup, K., Snellen, I., Sobiecki, M., Soret, L., Sozzetti, A., Stiepen, A., Strugarek, A., Taylor, J., Taylor, W., Terenzi, L., Tessenyi, M., Tsiaras, A., Tucker, C., Valencia, D., Vasisht, G., Vazan, A., Vilardell, F., Vinatier, S., Viti, S., Waters, R., Wawer, P., Wawrzaszek, A., Whitworth, A., Yung, Y. L., Yurchenko, S. N., Zapatero Osorio, M. R., Zellem, R., Zingales, T., and Zwart, F., "A chemical survey of exoplanets with ARIEL," *Experimental Astronomy* **46**, 135–209 (Nov. 2018).

[2] Tinetti, G., Eccleston, P., Lueftinger, T., Pilbratt, G., and Puig, L., "Ariel Phase B," in [*European Planetary Science Congress*], EPSC2020–696 (Sept. 2020).

[3] Lueftinger, T., Tinetti, G., Ecclestone, P., Salvignol, J.-C., Fahmy, S., Lagage, P.-O., Micela, G., Pallé, E., Panic, O., Pascale, E., Vandenbussche, B., and Venot, O., "Ariel - The ESA M4 Space Mission to Focus on the Nature Of Exoplanets," in [*European Planetary Science Congress*], EPSC2021–610 (Sept. 2021).

[4] Pace, E., Tozzi, A., Abreu, M. A., Alonso, G., Barroqueiro, B., Bianucci, G., Bocchieri, A., Brienza, D., Brucalassi, A., Burresi, M., Canestrari, R., Carbonaro, L., Castanheira, J., Chioetto, P., Colomé Ferrer, J., Compostizo, C., Cortecchia, F., D'Anca, F., Del Vecchio, C., Diolaiti, E., Eccleston, P., Fahmy, S., Fernandez Soler, A., Ferruzzi, D., Focardi, M., Freitas, S., Galy, C., Garcia Perez, A., Gottini, D., Grella, S., Grisoni, G., Guerriero, E., Halain, J.-P., Hellin, M.-L., Ianni, L., Iuzzolino, M., Jollet, D., Lombini, M., Machado, R., Malaguti, G., Mazzoli, A., Micela, G., Miceli, F., Mondello, G., Morgante, G., Mugnai, L., Naponiello, L., Noce, V., Pascale, E., Perez Alvarez, J., Piazzolla, R., Pompei, C., Preti, G., Roose, S., Salatti, M., Salvignol, J.-C., Scippa, A., Serre, C., Simoncelli, C., Teixeira, F., Terenzi, L., Tinetti, G., Tommasi, L., Tommasi Di Vigano, E., Vandenbussche, B., Vernani, D., and Zuppella, P., "The telescope assembly of the Ariel space mission," in [*Space Telescopes and Instrumentation 2022: Optical, Infrared, and Millimeter Wave*], Coyle, L. E., Matsuura, S., and Perrin, M. D., eds., *Society of Photo-Optical Instrumentation Engineers (SPIE) Conference Series* **12180**, 1218011 (Aug. 2022).

[5] Del Vecchio, C., Carbonaro, L., Brucalassi, A., Tozzi, A., Gottini, D., Scippa, A., Pace, E., Malaguti, G., Micela, G., Morgante, G., Focardi, M., Pascale, E., Preti, G., Zuppella, P., Salatti, M., Piazzolla, R., Tommasi Di Vigano, E., Naponiello, L., and Chioetto, P., "Optimization of the Ariel primary mirror," in [*Space Telescopes and Instrumentation 2022: Optical, Infrared, and Millimeter Wave*], Coyle, L. E., Matsuura, S., and Perrin, M. D., eds., *Society of Photo-Optical Instrumentation Engineers (SPIE) Conference Series* **12180**, 1218041 (Aug. 2022).

[6] Gottini, D., Pace, E., Tozzi, A., Bianucci, G., Bocchieri, A., Brienza, D., Brucalassi, A., Canestrari, R., Carbonaro, L., Chioetto, P., Cortecchia, F., Del Vecchio, C., Diolaiti, E., Eccleston, P., Fahmy, S., Ferruzzi, D., Galy, C., Grisoni, G., Guerriero, E., Halain, J.-P., Hellin, M.-L., Iuzzolino, M., Jollet, D., Lombini, M., Malaguti, G., Micela, G., Missaglia, N., Morgante, G., Mugnai, L., Naponiello, L., Pascale, E., Piazzolla, R., Preti, G., Roose, S., Salatti, M., Salvignol, J.-C., Scippa, A., Terenzi, L., Tinetti, G., Tommasi Di Vigano, E., and Zuppella, P., "FEA testing the pre-flight Ariel primary mirror," in [*Space Telescopes and Instrumentation 2022: Optical, Infrared, and Millimeter Wave*], Coyle, L. E., Matsuura, S., and Perrin, M. D., eds., *Society of Photo-Optical Instrumentation Engineers (SPIE) Conference Series* **12180**, 1218042 (Aug. 2022).

[7] Tozzi, A., Brucalassi, A., Canestrari, R., Chioetto, P., Del Vecchio, C., Carbonaro, L., Cortecchia, F., Diolaiti, E., Eccleston, P., Falcini, G., Ferruzzi, D., Gottini, D., Guerriero, E., Iuzzolino, M., Lilli, R., Lombini, M., Malaguti, G., Micela, G., Miceli, F., Morgante, G., Pace, E., Pascale, E., Piazzolla, R., Preti, G., Salatti, M., Scippa, A., Tinetti, G., Tommasi, E., Vernani, D., and Zuppella, P., "Toward ARIEL's primary mirror," in [*Space Telescopes and Instrumentation 2022: Optical, Infrared, and Millimeter Wave*], Coyle, L. E., Matsuura, S., and Perrin, M. D., eds., *Society of Photo-Optical Instrumentation Engineers (SPIE) Conference Series* **12180**, 1218040 (Aug. 2022).